Supplementary Information

# Nanoscale characterization of DNA conformation using dual-color fluorescence axial localization and label-free biosensing

*Xirui Zhang,[a] George G. Daaboul,[b] Philipp S. Spuhler,[a] David S. Freedman,[b] Abdulkadir Yurt,[c] Sunmin Ahn,[a] and M. Selim Ünlü*[*a,b]*

[a]Department of Biomedical Engineering, Boston University, 44 Cummington St., Boston, MA 02215

[b]Department of Electrical and Computer Engineering, Boston University, 8 Saint Mary's St., Boston, MA 02215

[c]Division of Materials Science and Engineering, Boston University, 15 Saint Mary's St., Brookline, MA 02446

*Corresponding author: selim@bu.edu

Contents

1. Oligonucleotide sequences and nomenclature (Table S1).
2. Uniform and consistent spot morphology of DNA microarrays on the polymer surface (Figure S1).
3. Schematic illustration of customized flow cell assembly (Figure S2).
4. Simulation of the deviation of fluorophore axial heights from expected values on substrates with different SiO2 thicknesses (Figure S3, Figure S4).
5. Calculation of the average orientation of surface-immobilized dsDNA (Figure S5, Figure S6).
6. Validating the dual-color SSFM system with nanometer scale surface steps (Figure S7, Figure S8, Figure S9)
7. Simulation of the deviation of axial step heights from expected values using dual-color SSFM (Figure S10).
8. References

## 1. DNA sequences

Table S1. DNA sequences and nomenclature

| Name | Sequence |
|---|---|
| **60-bp dsDNAs** | |
| Seq1 (Scheme1) | 5'-GCT GTT AGA AGA TAG GGC CAA AAA AGC ATT GCT TAT CAA TTT GTT GCA CCT GAC CGA TGA-3'-C6-$NH_2$ |
| Complement | 5'-Atto647N-TCA TCG GTC AGG TGC AAC AAA TTG ATA AGC AAT GCT TTT TTG GCC CTA TCT TCT AAC AGC-3' |
| Seq2 (Scheme2) | $NH_2$-C6-5'-GCT GTT AGA AGA TAG GGC CAA AAA AGC ATT GCT TAT CAA TTT GTT GCA CCT GAC CGA TGA-3' |
| Complement | 5'-Atto647N-TCA TCG GTC AGG TGC AAC AAA TTG ATA AGC AAT GCT TTT TTG GCC CTA TCT TCT AAC AGC-3' |
| Seq3 | 5'-GCT GTT AGA AGA TAG GGC CAA AAA AGC ATT GCT TAT CAA TTT GTT GCA CCT GAC CGA TGA-3'-C6-$NH_2$ |
| Complement | 5'-Atto532-TCA TCG GTC AGG TGC AAC AAA TTG ATA AGC AAT GCT TTT TTG GCC CTA TCT TCT AAC AGC-3' |
| Seq4 | $NH_2$-C6-5'-GCT GTT AGA AGA TAG GGC CAA AAA AGC ATT GCT TAT CAA TTT GTT GCA CCT GAC CGA TGA-3' |
| Complement | 5'-Atto532-TCA TCG GTC AGG TGC AAC AAA TTG ATA AGC AAT GCT TTT TTG GCC CTA TCT TCT AAC AGC-3' |
| Seq5 (Scheme3) | 5'-Atto647N-GCT GTT AGA AGA TAG GGC CAA AAA AGC ATT GCT TAT CAA TTT GTT GCA CCT GAC CGA TGA-3'-C6-$NH_2$ |
| Complement | 5'-Atto532-TCA TCG GTC AGG TGC AAC AAA TTG ATA AGC AAT GCT TTT TTG GCC CTA TCT TCT AAC AGC-3' |
| Seq6 (Scheme4) | 5'-Atto532-GCT GTT AGA AGA TAG GGC CAA AAA AGC ATT GCT TAT CAA TTT GTT GCA CCT GAC CGA TGA-3'-C6-$NH_2$ |
| Complement | 5'-Atto647N-TCA TCG GTC AGG TGC AAC AAA TTG ATA AGC AAT GCT TTT TTG GCC CTA TCT TCT AAC AGC-3' |
| **20-bp dsDNA** | $NH_2$-C6-5'-iCy5/GCT GTT AGA AGA TAG GGC CA |
| Complement | 5'-Atto532N-TGG CCC TAT CTT CTA ACA GC |
| **40-bp dsDNA** | $NH_2$-C6-5'-iCy5/ATC TGA ACC CAC CGC TAT TCC ATG CAC TTG ATT CCG AGG C |
| Complement | 5'-Atto532N-CCT CGG AAT CAA GTG CAT GGA ATA GCG GTG GGT TCA GAT |

We chose Atto532 (green) and Atto647N (red) fluorophores to label oligonucleotides for dual-color SSFM because their excitation wavelengths and emission spectrums are compatible with normal fluorescent microscopes. Also, they have excellent photostability, and their emission spectrums are distinctly separate, which allows for accurate spectral fitting.

## 2. Uniform and consistent spot morphology of DNA microarrays prepared on the polymer surface

We obtained consistent spot morphology by optimizing spotting conditions, such as spotting concentration, temperature and humidity. Spectrum measurements were made on the center of each DNA spot where each laser beam and the pinhole image were focused. All spots used in experiments possessed uniform morphology within measured area, defined by the diffraction limit of the laser beams and the image of the pinhole with a diameter of 20 μm (Diameter of pihole/5x objective magnification). Averages of the fluorophore heights and thicknesses of DNA molecules reside within the measured area were quantified.

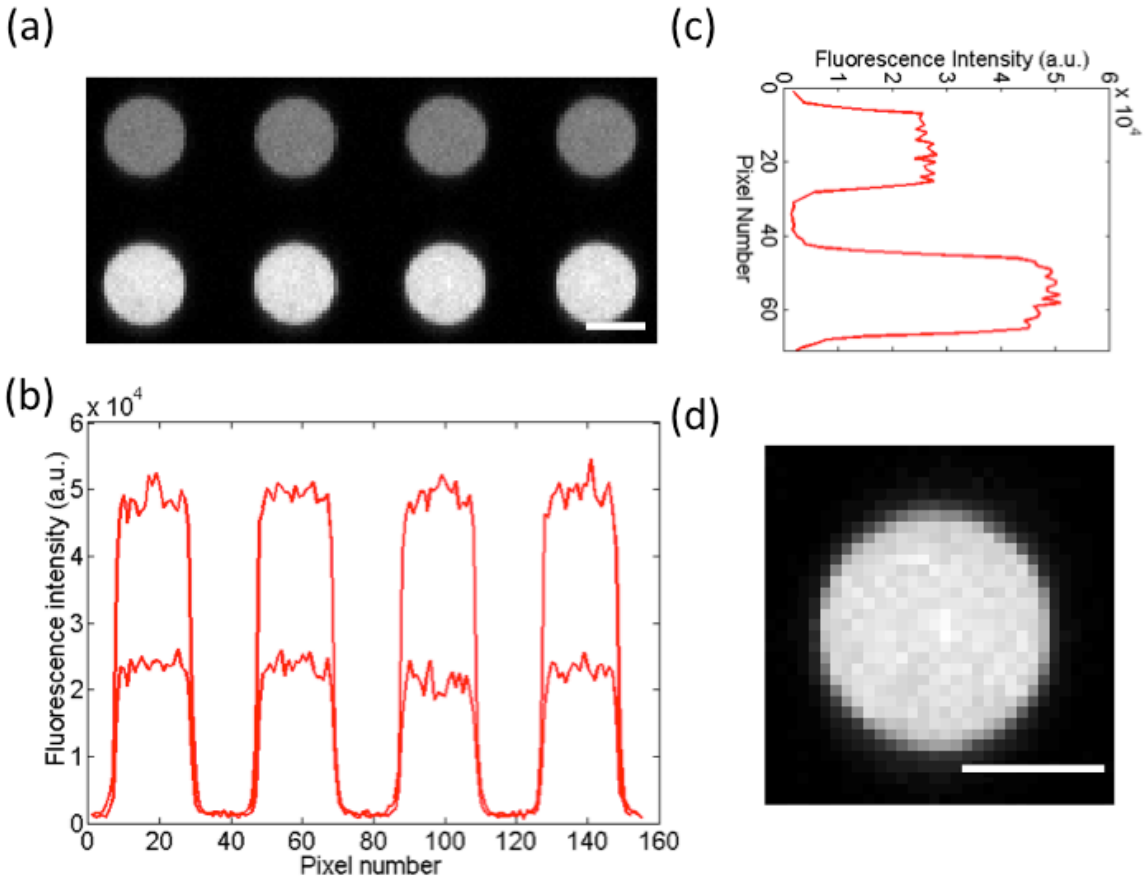


Figure S1. Uniform and consistent DNA spot morphology on the polymer surface. (a) A fluorescence image of example DNA spots immobilized on the polymer surface scanned by GenePix 4000B microarray scanner. The DNA molecules labeled with Atto647N are spotted at two concentrations, 5 μM and 10 μM. (b) Horizontal fluorescence intensity profile of eight DNA spots of two different densities. (c) Vertical fluorescence intensity profile of two DNA spots of different densities. The variability of fluorescence intensity within each spot is less than 10%, showing spotting is consistent from spot to spot. (d) Zoomed in fluorescence image of one DNA spot. Scale bar shows a distance of 100 μm.

### 3. Customized flow cell assembly

All measurements were made on chips fixed in the flow cell as described in the Figure S2. The height of the flow cell is 1 mm, the length of the flow cell is 20 mm, and the width of the flow cell is 5 mm. In dry measurements, the chip resided in air in the flow cell. In wet measurements, such as all the DNA orientation and hybridization measurements, the chip was immersed in buffer solution. Each buffer solution was driven by a peristaltic pump into and out of flow cell through the inlet and outlet via stainless steal and non-shedding silicon tubing and tubing connecters.

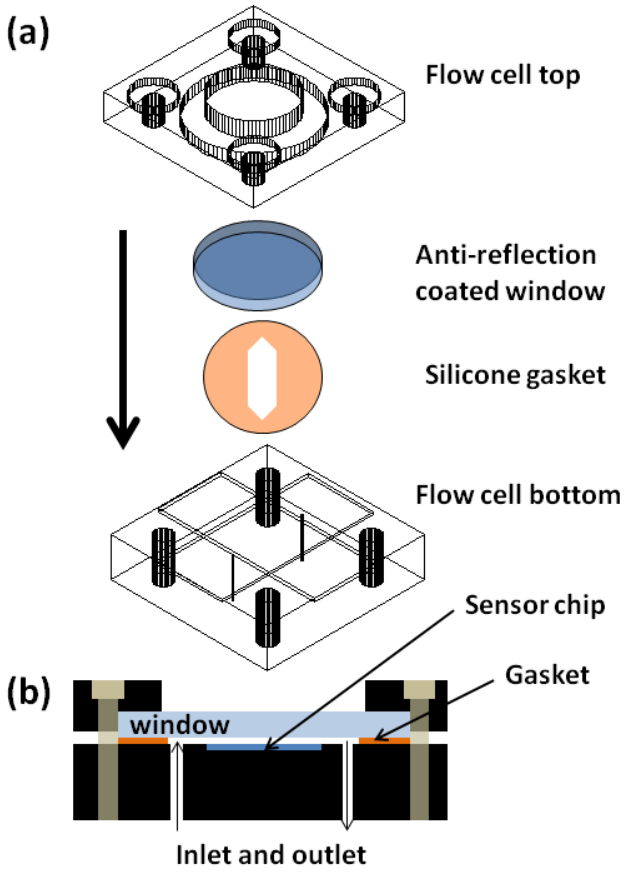


Figure S2. Customized flow cell assembly. (a) Four different components of the flow cell are presented and assembled from top to bottom as indicated by the black arrow. (b) Cross section of an assembled flow cell with the SSFM chip (dark blue) fixed in place is shown.

## 4. Simulation of the deviation of fluorophore axial heights from expected values on substrates with different $SiO_2$ thicknesses

We simulated the deviation of fluorophore axial heights determined by dual-color SSFM from expected values using different $SiO_2$ thicknesses under the usable green and red fluorescence and LED spectral bandwidths. We determined the usable bandwidth of each spectrum by the wavenumbers at which the transmission of the filters are larger than 90% or the fluorescence or LED intensity is larger than 50% of its maximum. Thus the usable bandwidth of red fluorophore is 700 $cm^{-1}$, that of green fluorophore is 450 $cm^{-1}$, and that of LED is 800 $cm^{-1}$. Figure S3 shows the emission spectrums of the fluorophores and the LED and the passbands of the dichroic beam splitters and laserline notch filters.

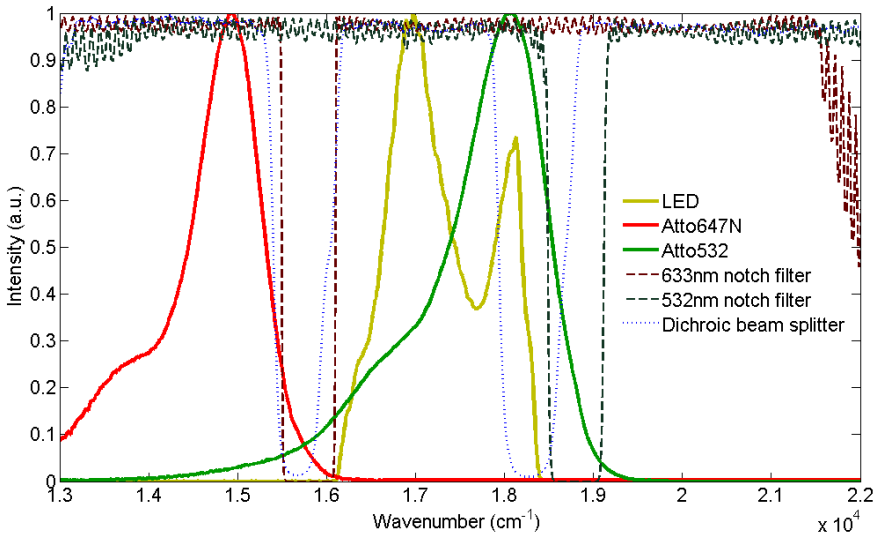


Figure S3. The emission spectrums of the fluorophores and the LED used in dual-color SSFM. The usable bandwidth of each spectrum is constrained by the passbands of the notch filters and the dichroic beam splitters shown as dashed and dotted lines.

Fluorescence interference spectrums were generated by assuming a certain $SiO_2$ thickness and modeling the fluorophores as classical dipoles on a layered reflecting surface[1]. The interference spectrums were scaled by the emission spectral envelops of the fluorophores given by the manufacturer. Shot noise of the CCD camera following a Poisson distribution was also added to the spectrum. The simulated fluorescence interference spectrums were fit to a custom SSFM algorithm and the average axial fluorophore heights were determined to be the values with the Lease Square Fitting errors. Figure S4(a) shows the mean deviation of the fitted fluorophore

axial heights from initial set values in 10 simulations as a function of the number of oscillations in the spectral bandwidth. The number of oscillations within the limited spectral bandwidth is proportional to the $SiO_2$ layer thicknesses (Figure S4(b)). The results show that at a $SiO_2$ layer thicknesses of 17 μm, we can obtain at least two periods of oscillations in each available spectral bandwidth of dual-color SSFM, corresponding to less than 0.3 nm deviation of fluorophore height determination. The same analysis applies to the LED interference spectrum. The relationship between number of interference oscillations and $SiO_2$ layer thicknesses remains the same for LED-RS. Since the available bandwidth of the LED spectrum is wider than that of the fluorophores, the determined $SiO_2$ layer thicknesses for dual-color SSFM is also applicable for LED-RS.

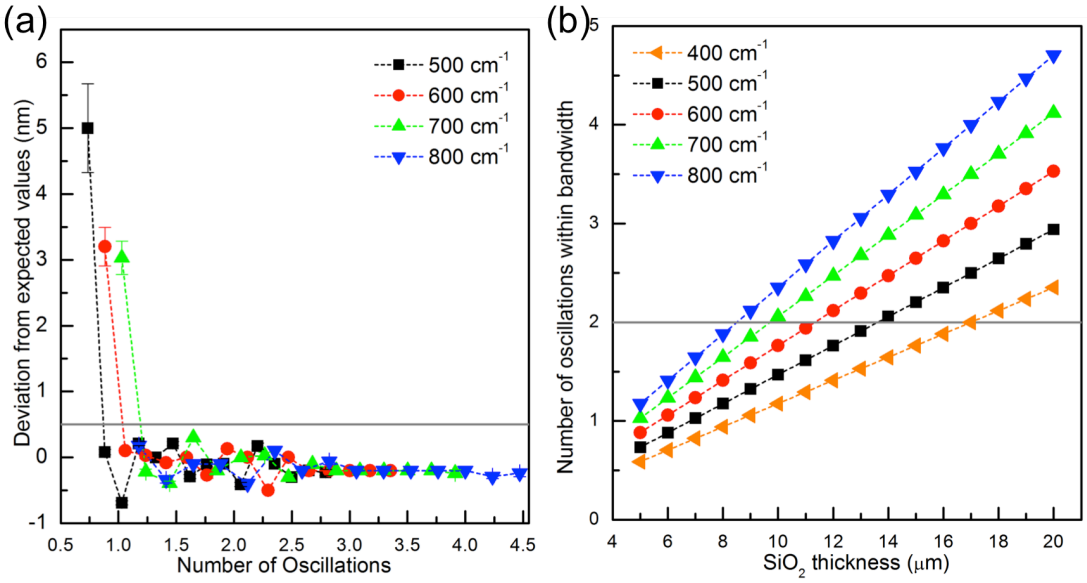


Figure S4. (a) The simulated mean deviation of fluorophore axial heights from expected values on $SiO_2$ layers of different thicknesses using different spectral bandwidths. The mean deviation is obtained from 10 simulated fitting results. (b) Number of interference oscillations within each spectral bandwidth on SSFM substrate is proportional to the $SiO_2$ thicknesses. Gray lines are guides for the eye as reference thresholds.

**5. Calculation of the orientation of double-stranded DNA (dsDNA):**

To calculate the average orientation (θ) of dsDNA molecules whose fluorescence signals are collected in one measurement, we used a simple trigonometric model. As the contour length of the dsDNA used in experiments (20bp, 40bp, and 60bp) is much shorter than its persistence length (about 50nm[2]), we model each dsDNA molecule as a rigid rod tethered to the surface on a pivot. The other end of each dsDNA molecule can rotate around the pivot at various orientations to the surface. If we consider each orientation of the dsDNA to the surfaces as an energy state, the hemisphere shown in Figure S5 illustrates all the states possibly accessible by the dsDNA molecule on a planar surface. Without any constraints, the probability distribution function of the orientations of each dsDNA molecule[3,4] is:

$$f(\theta) = \frac{cos(\theta)}{\int_0^{\frac{\pi}{2}} cos(\theta)\, d\theta} = \cos(\theta), \left(0 \le \theta \le \frac{\pi}{2}\right)$$

Thus, the mean orientation of a dsDNA molecule in random rotation under thermal fluctuation or the mean orientation of large number of dsDNA molecules is:

$$\langle\theta\rangle = \int_0^{\pi/2} \theta\, f(\theta\,) d\theta = 33°$$

The upper limit of the integration represents the maximum polar angle (the complement of the minimum orientation to surface) accessible for the dsDNA molecules on a 2-D surface. According to Manning's counterion condensation theory, dsDNA is inherently negatively charged in electrolyte solutions with equally spaced (0.34 nm) negative point charges[5]. Thus due to electrostatic repulsion and steric hindrance, closely tethered dsDNA molecules may rotate with smaller than 90° maximum polar angles, resulting in average orientations higher than 33°.

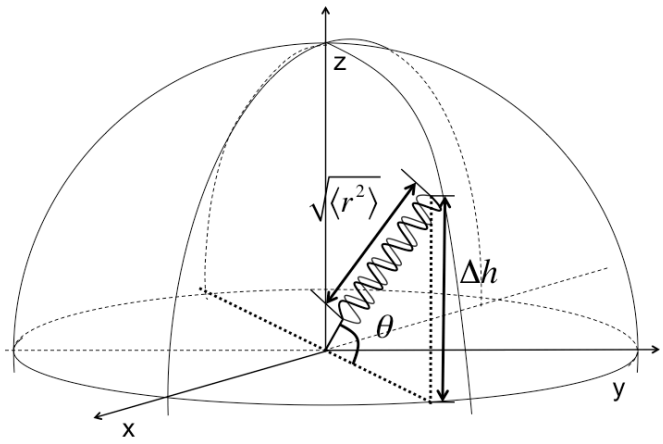


Figure S5. A dsDNA molecule is modeled as a rigid rod with an orientation θ to the surface. $\sqrt{\langle \mathbf{r^2} \rangle}$ is the root-mean-square of the end-to-end distance of dsDNA under experimental conditions. ∆h is the axial height difference between the surface-distal end and surface-proximal end of the dsDNA. The hemisphere illustrates the orientations accessible by an unconstrained dsDNA molecule in random t rotation under thermal fluctuations around the pivot on a 2-D surface.

The average orientation of many dsDNA molecules can be calculated as $\langle\theta\rangle = \arcsin(\Delta h/\sqrt{\langle r^2\rangle})$. $\sqrt{\langle \mathrm{r}^2 \rangle} = \sqrt{2l^2(L/l - 1 + e^{-L/l})}$ is the root-mean-square of the end-to-end distance of dsDNA, $l$ is the persistent length of dsDNA, $L$ is the contour length, and $\Delta h$ is the axial height between the surface-proximal and surface-distal fluorophores on each dsDNA molecule. Since our spectral axial localization method only renders the ensemble average axial height difference ($\langle\Delta h\rangle$), we approximate the mean orientation of the dsDNA molecules detected in one measurement of one dsDNA spots as $\theta = \arcsin(\langle\Delta h\rangle/\sqrt{\langle r^2\rangle})$. A simulated analysis shows that this approximation underestimates $\langle\theta\rangle$ by 2-3 degrees (Figure S6).

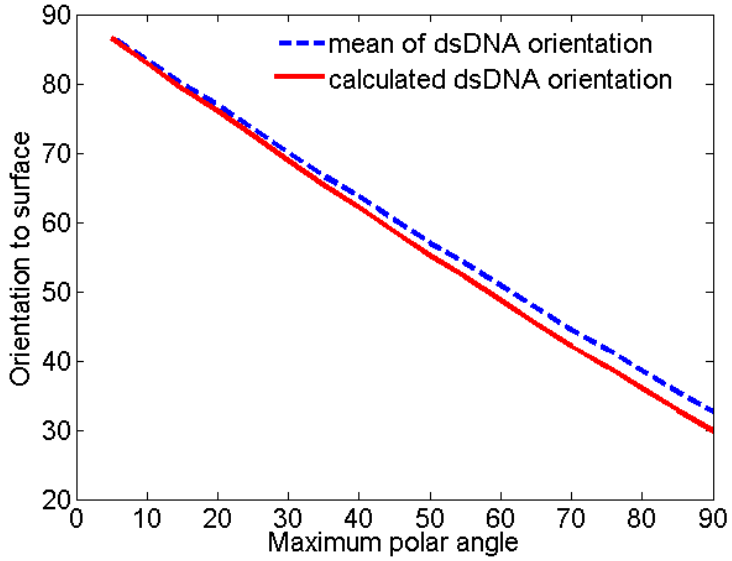


Figure S6. Approximation of the mean of dsDNA orientation with calculated average orientation of dsDNA spot using ensemble average height difference $\langle \Delta \boldsymbol{h} \rangle$ measured by dual-color SSFM.

**6. Validating the dual-color SSFM system with nanometer scale steps:**

To show that the dual-color SSFM can determine fluorophore heights with comparable accuracy as single-color SSFM, we also measured heights of nanometer scale steps on the surface of the chip. The steps were fabricated by patterning the chips with standard photolithographic techniques followed by etching in diluted buffered oxide etch (BOE). The etching was carried out for different time periods (5 min, 8 min, and 10 min) to create nanometer scales steps of different heights. The chips were then coated with the polymer and spotted at 500 μm pitch with dsDNA molecules tagged with both Atto532 (green fluorophores) and Atto647N (red fluorophores). We scanned a line profile of the surface of each chip in both dry (air) and wet conditions (Tris buffer: 10 mM Tris, 50 mM NaCl, pH 7.6). The step height was calculated by averaging the difference of the fluorophore heights to the $SiO_2$/Si interface on the left side from those on the right side. We measured the step height with both the red and green modality of SSFM. We also validated the results with LED-RS measurements. For both dry and wet conditions, the step heights measured by SSFM and LED-RS matched each other to within one nanometer (Figure S7, Figure S8, Figure S9(b)). The results were also consistent with the

estimated heights of the etched steps based on the etch rate characterized separately by an Interferometric Reflectance Imaging Sensor (IRIS)[6] (Figure S9).

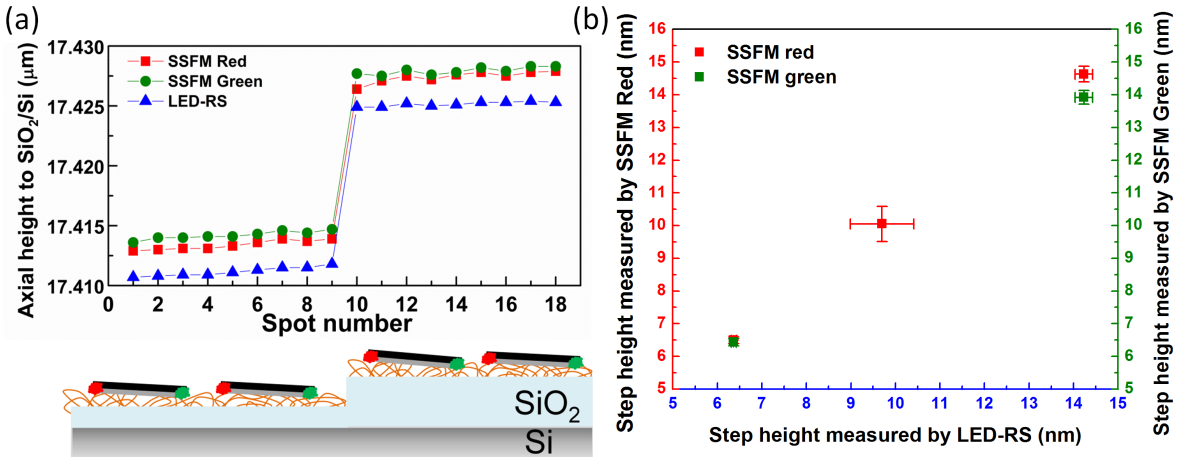


Figure S7. Measurements of chips with nanometer scale steps on the surface with dual-color SSFM and LED-RS. (a) An example of the measured surface profile of an etched chip. Eighteen spots of dsDNA labeled with both green and red fluorophores pitched at 500 μm on the substrate were measured both in dry (shown in this figure) and in solution (wet) (Figure S8). The average step height was calculated by subtracting the average fluorophore heights of dsDNA spots on the left side from those on the right side of the chip. A schematic illustration of the one-dimensional etching profile of the step with labeled dsDNA molecules immobilized is shown at the bottom (not to scale). (b) The measured step heights of the etched chips separately immersed in BOE for 5 min, 8 min and 10 min. The results of each color modality of SSFM match with the step heights measured with LED-RS within one nanometer. The dsDNA immobilized on the chip etched for 10 min did not have green fluorophores.

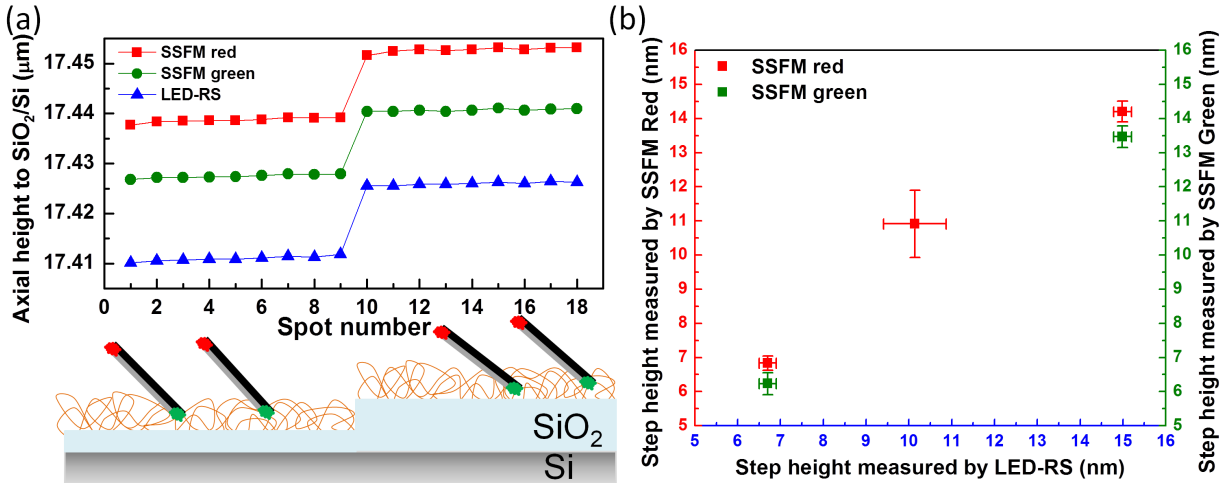


Figure S8. Measurements of chips with nanometer scale steps on the surface with dual-color SSFM and LED-RS in solution. (a) Same SSFM chip with dsDNA spots was immersed in buffer. The polymer surface swells upon hydration, elevating and orienting the dsDNA. Thus, the red fluorophore at the distal end is higher than the green fluorophore at the proximal end of the dsDNA. (b) The measured step heights of the etched chips separately immersed in BOE for 5 min, 8 min and 10 min by dual-color SSFM and LED-RS. The results of each color modality of SSFM match with the step heights measured with LED-RS within one nanometer in solution. The dsDNA immobilized on the chip etched for 10 min did not have green fluorophores.

We patterned IRIS substrates with an array of circular etched spots of 100 μm in diameter by photolithography. The etched spots were created in the same BOE solution for different lengths of time. The chips were cleaned with the same procedure described in the Experimental section. An IRIS image was taken of each chip and the absolute height of each pixel was obtained from the IRIS fitting algorithm. The etched step height was calculated as the average of 10 spot height differences between the average absolute height inside the spot and that of an annuli area outside the spot. We estimate an approximate etching rate of about 1.5 $nm \cdot min^{-1}$ on the IRIS substrates, very close to the etching rate of 1.4 $nm \cdot min^{-1}$ measured on SSFM substrates by LED-RS and SSFM (Figure S9).

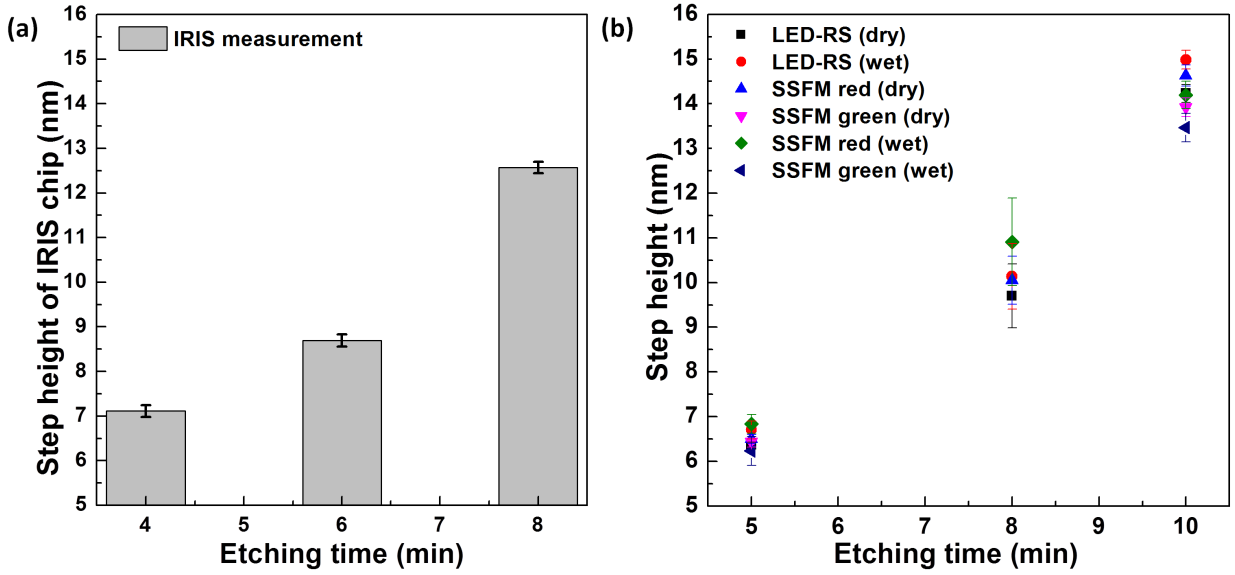


Figure S9. (a) Average step heights of circular etched spots measured on IRIS substrates. Patterned IRIS chips were separately etched in 60:1 diluted BOE for 4 min, 6 min, and 8min. The results are average values for the etched step heights of 10 spots measured by IRIS. (b) Step heights of SSFM chips separately etched in BOE for 5 min, 8 min and 10 min. The results were measured by dual-color SSFM and LED-RS in both air (dry) and solution (wet). The results of each color of SSFM match with the step heights measured with LED-RS. The step height measurements of SSFM in solution have larger variance due to the dependence of dsDNA orientation on varied surface immobilization density.

## 7. Simulation of the deviation of axial step heights from expected values using dual-color SSFM

We simulated the deviation of axial step heights determined by dual-color SSFM from expected values ranging from 2 nm to 100 nm on substrates of different $SiO_2$ thicknesses. Red fluorophores were assumed to be at a lower axial height than green fluorophores. Fluorescence interference spectrums were generated as described in section 4. The step height was obtained by subtracting the average axial height of red fluorophores from that of the green fluorophores. Both axial heights were determined using the same fitting method as in section 4. The simulation shows that the system can determine height differences for a wide range on SSFM substrates with sub-nanometer accuracy.

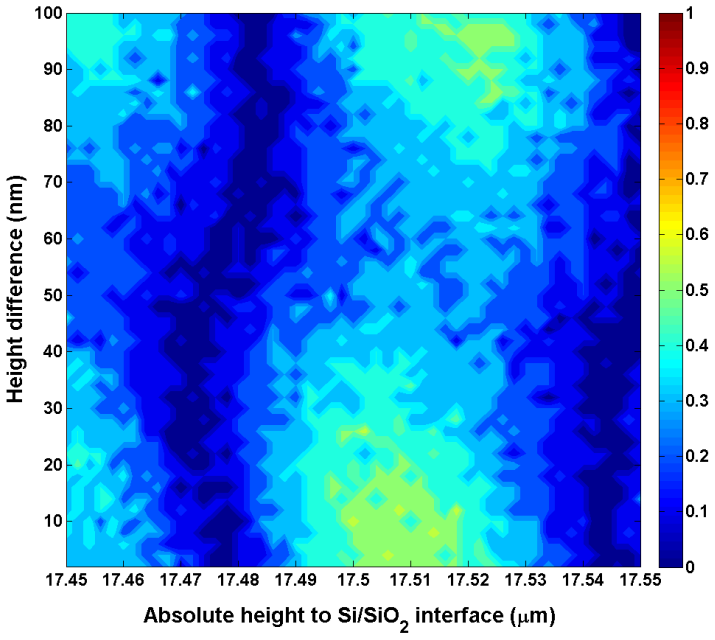


Figure S10. Simulation of the determination of various step heights ranging from 2 nm to 100 nm on substrates of different $SiO_2$ thicknesses. Red fluorophores are assumed to be at lower axial height than green fluorophores. The color scale shows the deviation of the axial height difference determined by dual-color SSFM are mostly less than half of a nanometer in the simulation.

## 8. References


1. L. Moiseev, C. R. Cantor, M. I. Aksun, M. Dogan, B. B. Goldberg, A. K. Swan, and M. S. Ünlü, *J. Appl. Phys.*, 2004, **96**, 5311.
2. Y. Lu, B. Weers, and N. C. Stellwagen, *Biopolymers*, 2002, **61**, 261–275.
3. U. Rant, K. Arinaga, S. Fujita, N. Yokoyama, G. Abstreiter, and M. Tornow, *Org. Biomol. Chem.*, 2006, **4**, 3448.
4. P. S. Spuhler, L. Sola, X. Zhang, M. R. Monroe, J. T. Greenspun, M. Chiari, and M. S. Ünlü, *Anal. Chem.*, 2012, **84**, 10593–10599.
5. G. S. Manning, *Biophysical chemistry*, 2002, **101**, 461–473.
6. G. G. Daaboul, R. S. Vedula, S. Ahn, C. A. Lopez, A. Reddington, E. Ozkumur, and M. S. Ünlü, *Biosensors and Bioelectronics*, 2011, **26**, 2221–2227.